Available online at www.sciencedirect.com

ScienceDirect

Procedia Structural Integrity 42 (2022) 847–856

Structural Integrity Procedia

www.elsevier.com/locate/procedia

23 European Conference on Fracture - ECF23

Side-groove effect on fracture mechanical fatigue testing of PLA material

Aleksa Milovanović[a*], Jan Poduška[b], Lukaš Trávníček[b,c], Luboš Náhlík[b], Aleksandar Sedmak[d], Miloš Milošević[a], Filippo Berto[e]

[a]*University of Belgrade, Innovation Center of The Faculty of Mechanical Engineering, Kraljice Marije 16 street, Belgrade 11120, Serbia*
[b]*Institute of Physics of Materials, Academy of Sciences of the Czech Republic, Žižkova 22, Brno 61662, Czech Republic*
[c]*CEITEC BUT, Brno University of Technology, Purkyňova 123, Brno 62100, Czech Republic*
[d]*University of Belgrade, Faculty of Mechanical Engineering, Kraljice Marije 16 street, Belgrade 11120, Serbia*
[e] *Norwegian University of Science and Technology (NTNU), Richard Birkelands vei 2b, Trondheim 7491, Norway*

Abstract

PLA polymer is probably the most used thermoplastic material in FDM technology nowadays. Besides prototyping purposes, FDM materials are also considered for functional application use, thanks to the fast fabrication of components, relatively simple workflow, and the absence of material waste that this technology offers. Except for static material properties, data concerning the expected lifetime and reliability of AM parts under cyclic loading are also necessary for functional purposes. Due to the exceptional structural complexity of FDM parts, minor modifications in material testing must be used sometimes. The subject of this paper is the fracture mechanics-based fatigue testing of CT specimens that results in crack kinetics description like the Paris' law. One of the objectives is also to describe the effect of SGs placed on the surface of CT specimens, and the effect of different layer heights. The main intention of the SGs is to secure a straight crack propagation path, thus imposing the crack to follow the Mode I condition, predominantly. A set of regular CT specimens and specimens with SGs was prepared with a full infill density interior and with different layer heights (0.1 mm and 0.3 mm). Crack kinetics measured on these specimens are presented in this paper and discussed.

Peer-review under responsibility of the scientific committee of the 23 European Conference on Fracture – ECF23

Keywords: Side-grooves; Fracture mechanical fatigue; PLA material.

* Corresponding author. Tel.: +381-64-614-8698.
E-mail address: amilovanovic@mas.bg.ac.rs

Peer-review under responsibility of the scientific committee of the 23 European Conference on Fracture – ECF23
10.1016/j.prostr.2022.12.107

1. Introduction

FDM is one of the most utilized AM technologies today and is based on the extrusion of a molten thermoplastic material onto a build platform, thus creating a physical model in a layer-by-layer fashion. FDM materials are created and shipped to customers in form of a round filament. Such filament is fed into an extruder mechanism on the FDM machine, where it is heated above the melting point, and finally extruded onto a build platform, as described thoroughly by Milovanović et al. (2020). Thermoplastic materials used in FDM are PLA, ABS, PET, etc. PLA has a significant advantage over the other FDM thermoplastics, due to its natural origin and biodegradability (DeStefano et al. (2020), Pawar et al. (2014), Ebrahimi et al. (2022)). Also, PLA is one of a few FDM thermoplastics that has been approved by the Food and Drug Administration for commercial use (Petersmann et al. (2020)). Nowadays PLA material is used for prototyping purposes and some functional applications where it should replace petroleum-based thermoplastics (Farah et al. (2016)), but the most interesting research topic in which PLA is involved is its possible biomedical use. Because of its biocompatibility and biodegradability, this material is still in research for potential applications, such as bone scaffolds, stents, screws, etc. (DeStefano et al. (2020), Pawar et al. (2014), Ebrahimi et al. (2022), Petersmann et al. (2020)). The possibility, that 3D-printed PLA is going to be used to make these, often load-bearing, mechanical parts, requires knowledge about its capacity in terms of fatigue and fracture.

The FDM parts inherit various mechanical properties depending on the chosen technological parameters that can be set for the manufacturing process, such as building direction, raster orientation, layer thickness, infill density, infill pattern, extrusion and bed temperature, etc. In general, the mechanical properties of FDM parts are inferior to their compression-molded counterparts and they have a strongly anisotropic character due to weak inter-layer bonds (Song et al. (2017), Spoerk et al. (2017)).

Nomenclature

PLA	Polylactic Acid
FDM	Fused Deposition Modeling
AM	Additive Manufacturing
CT	Compact Tension (specimen)
SG	Side-Groove
ABS	Acrylonitrile Butadiene Styrene
PET	Polyethylene Terephthalate
C	Material constant in the Paris law
m	Material constant in the Paris law – the exponent
W	Width of a CT specimen [mm]
a	Initial notch length in the CT specimen (including a pre-crack) [mm]
CAD	Computer-Aided Design
R	Cycle asymmetry ratio [-]
$\mathrm{d}a/\mathrm{d}N$	Crack growth rate [mm/cycle]
$K_{I,max}$	Stress intensity factor, max. value in the loading cycle [MPa·m$^{1/2}$]

The fatigue properties of FDM PLA in terms of S-N curves (or Woehler curves) were investigated in numerous studies (Ezeh & Susmel (2018), Ezeh & Susmel (2019), Afrose et al. (2016)), considering various technological parameters, to find the recommendations for the best possible outcome of FDM. To achieve the best mechanical properties and to provide the higher lifespan of an FDM component, infill density must be maximized. According to Jerez-Mesa et al. (2017) and Travieso-Rodriguez et al. (2020), the honeycomb infill pattern is the most beneficial for fatigue life. This claim coincides with findings in the Tissue Engineering field by Zhao et al. (2018) and Hutmacher et al. (2001). However, the highest structural response is influenced by layer thickness, i.e., final FDM parts have overall better cohesion between layers with lower layer heights, because of greater layer contact and smaller air gaps between them (Ezeh & Susmel (2019), Travieso-Rodriguez et al. (2020), Safai et al. (2019)). In addition to this

statement, Gomez-Gras et al. (2018) claim that for the same nozzle diameter it is better to use lower layer heights to improve adhesion between layers.

However, there are still scarce resources regarding fracture mechanical fatigue of FDM materials – i.e., description of actual crack kinetics in terms of either linear-elastic fracture mechanics or elastic-plastic fracture mechanics. Suitable information can be found for ABS (Alshammari et al. (2021), Azadi et al. (2021)), but for the PLA there has only been one comprehensive work by Arbeiter et al. (2018), where fracture mechanical fatigue tests on CT specimens were conducted. In this study, the material was near homogenous and isotropic thanks to parameter optimization according to Spoerk et al. (2017). The crack kinetics were described using the Paris law (Paris & Erdogan (1963)), obtained C and m values were merged for all fatigue-tested specimens and later used for lifetime estimation of an actual FDM structural component (Arbeiter et al. (2020)).

This paper aims to broaden the knowledge about the fracture mechanical fatigue of PLA. Crack growth rate measurements on CT specimens made of PLA under different printing conditions are described here. The specimens were manufactured with a hexagonal infill pattern with different layer heights. The main focus of the study was to investigate the role of a 3D-printed (not machined) SG in the actual measurements, because Valean et al. (2020) reported that printed notches provided lower data scatter than conventionally milled ones, due to process precision. Attention was paid also to the influence of different layer heights and the presence of voids on the applicability of the Paris law.

2. Materials and Methods

Regular and SGed CT specimens were prepared according to ASTM D5045-14 (2014) for $W = 50$ mm. Only the initial notch length a was not prepared according to the standard but it was reduced so that $a/W = 0.35$ to allow for a longer crack propagation as in Arbeiter et al. (2018). Regular CT specimens were 62.5×60×10 mm in bulk, and SGed CTs were 3 mm thicker. The SGs have a round shape, 3 mm in diameter, thus the minimal thickness of the SGed CT specimens was the same as the overall thickness of regular CT specimens. CAD models were created in SolidWorks software (Dassault Systèmes, France). CT specimen dimensions and SGed CT specimen geometry are shown in Fig. 1.

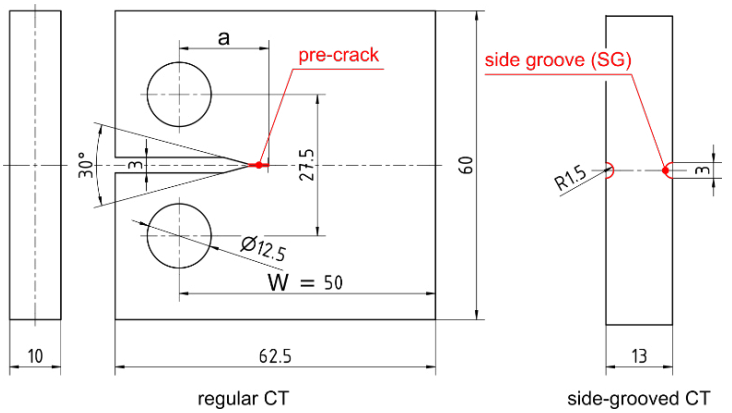

Fig. 1. CT specimen 2D dimensions (Left); SGed CT specimen geometry (Right) – the geometry is the same as the regular CT apart from the pictured SGs and the thickness.

All CT specimens were printed with the largest flat surfaces facing the build platform (Fig. 2-Left). Such flat-oriented FDM parts are supposed to have the highest stiffness and strength values according to Gao et al. (2022). Altogether, four batches were prepared, each containing four specimens. Two batches for the layer height of 0.3 mm (one batch regular, one with SGs) and two batches for 0.1 mm. The printing of the specimens was done using the hexagonal infill pattern, which resulted in a structure that contained regularly placed cavities. Although infill density was set to be 100 % for all specimens, air gaps are present in raster-to-raster locations due to the oval shape of the

material upon extrusion, and because those air gaps eventually widen shortly after the extruded material shirks toward its center, due to material cooling.

Specimens were then prepared for the actual fatigue testing. Their surfaces were ground on a metallographic grinder to make them smoother and to get rid of 3D printing surface textures. The detection of growing crack was going to be done optically by cameras. This procedure requires a smooth surface without any distinctive features. Also, in the first tested specimens, the front and back surface was sprayed with paint to try if the visibility of the crack gets better. Later, it was concluded that the grinding procedure was enough to secure sufficient crack visibility. Pre-cracks were machined using a metallographic sawmill of 0.4 mm blade thickness. The depth of the pre-crack was approximately 3-4 mm. The pre-crack length had to be longer than the outline thickness, as suggested by Milovanović et al. (2022). To make the experiments more precise, the total depth of the initial notch a, on both sides of the specimen, was measured using a microscope with a measuring table.

Fracture mechanical fatigue testing was performed on an Instron ElectroPuls® E3000 machine (Instron®, Norwood, MA, USA), with tests conducted at room temperature (Fig. 2-Right). The frequency of the load cycle was set to 10 Hz with cycle asymmetry of $R = 0.05$. There are suggestions in the literature to carry out fatigue tests of plastics at frequencies lower than 5 Hz (Safai et al. (2019)), because of the danger of hysteretic self-heating. However, 10 Hz is commonly reported as safe for the fatigue testing of PLA (Algarni et al. (2022), Ezeh & Susmel (2019), El Magri (2021)). One camera was placed on each side of the CT specimen, to monitor the crack propagation. After the conducted tests, fracture surfaces on CT specimens were examined by means of light microscopy using the Olympus SZX7 stereo microscope (Olympus, Japan).

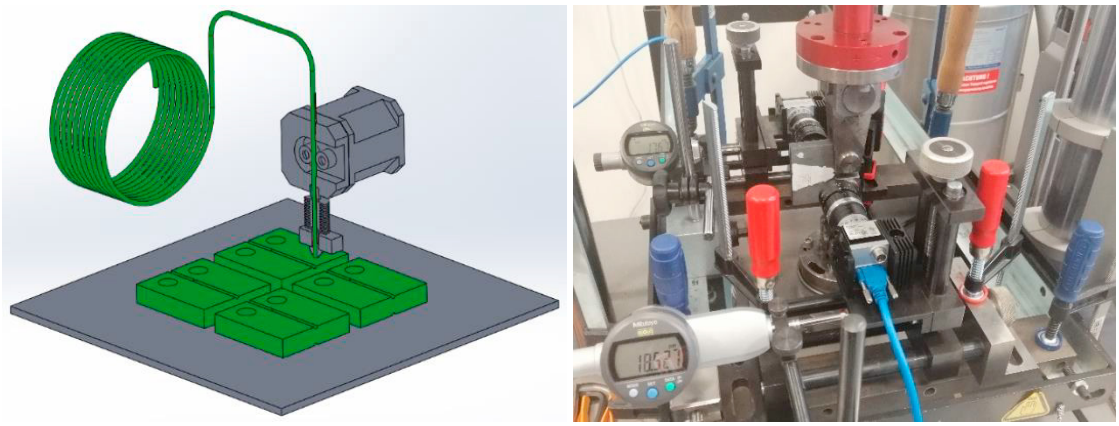

Fig. 2. Position of CT specimens on build platform (Left); Fracture mechanical fatigue testing setup (Right).

3. Results and Discussion

Fracture mechanical fatigue tests were first performed on the regular 0.3 mm CT specimens. Here, high structural inhomogeneity was present due to the application of the highest layer height, i.e., the lowest layer resolution during printing. The fracture surface of each CT specimen was observed using light microscopy (Fig. 3). In Fig. 3-Left, the most distinctive regions are labeled with numbers:

- *region 1*: nearly homogeneous outer layers, which cover the infill structure
- *region 2*: through-thickness holes in the infill structure
- *region 3*: the smooth surface of the pre-crack

Honeycomb structure was chosen as the infill type; thus, these through-thickness holes represent the interior of a single honeycomb. The layers covering the infill structure, from both the bottom and top sides, are nearly homogeneous and are usually manufactured with different raster orientations of the nozzle from the infill, as is the case here as well. In Fig. 3-Right it can be seen that the cracks were propagating in multiple directions depending on

the observed layer. In the surface layers, the direction was 45° and in the middle layers, which were printed in the honeycomb pattern, it was 30°. Based on these conclusions, there is a limit to the interpretation of the data, i.e., the followed crack was propagating mostly in the surface layers of the CT specimens, but that could be independent of the honeycomb layers on the inside.

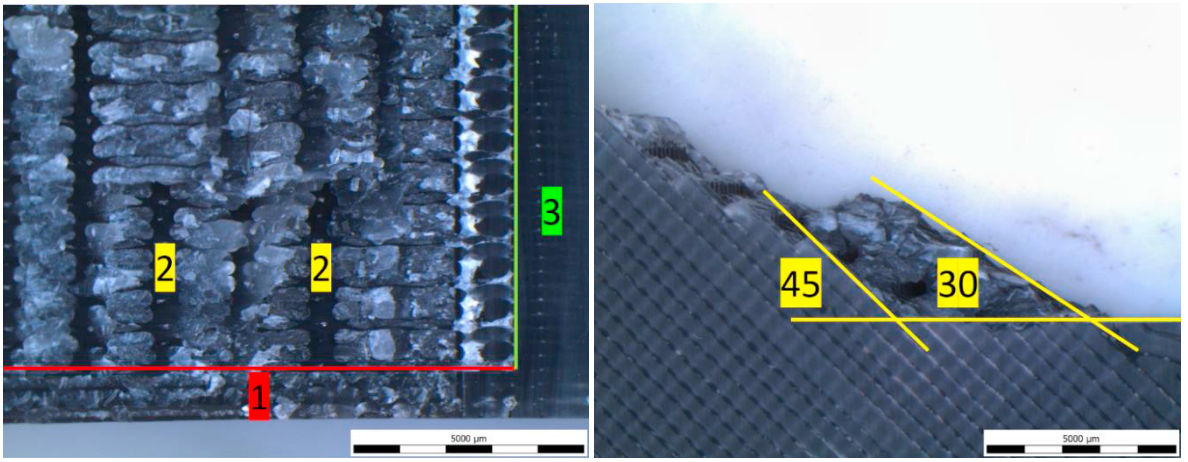

Fig. 3. Fracture surface of 0.3 mm regular CT specimen: Top view (Left); Side view (Right).

The main issue with regular 0.3 mm CT specimens was that the crack did not propagate in the middle plane. This creates a different kind of loading of the crack because instead of pure mode I (the opening mode) there is a mixture of mode I and the shear mode II which leads to unreliable results, when interpreting the data as mode I fracture.

It was one of the reasons to apply the SGs which should force the crack to propagate in the middle plane by increasing the constraint at the crack tip. As mentioned in the previous section, the SGs had a round shape, but when it comes to AM preparation, surface features have to be “layered”, and as such, the SGs received a stepwise shape (Fig. 4-Top). In the image, red lines show the borders of the lowest flat surface of the SG, at which the crack was observed during fatigue testing. In Fig. 4-Bottom, it can be seen that, in the actual tests, the crack initiated from the pre-crack and then continued to propagate behind one of the upper layers of the SG, which made it impossible to observe it and measure its length.

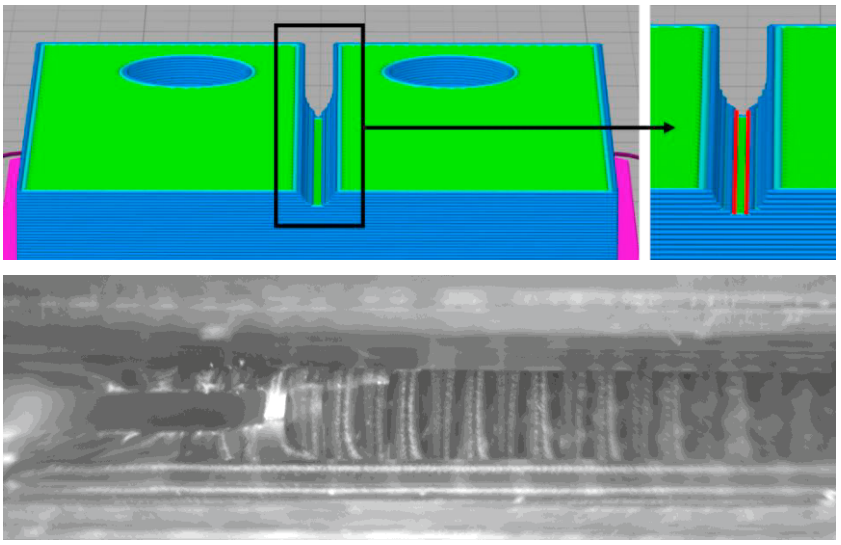

Fig. 4. SG stepwise shape in the slicer software (Top); Camera display from one of the tests (Bottom).

The light microscopy photos of the SG CT fracture surface show a notably layered structure of the SG on the top and bottom sides (Fig. 5-Left). In the side view (Fig. 5-Right), it can be seen that the crack was propagating either at the top edge of the SG or at the bottom edge during the test but kept a straight direction thanks to the SG. Hence, the SGs proved to be reliable for forcing the crack to propagate in the straight direction as expected, but at the same time, their layered structure created a sort of optical barrier, which is not ideal for the intended type of crack kinetics measurements.

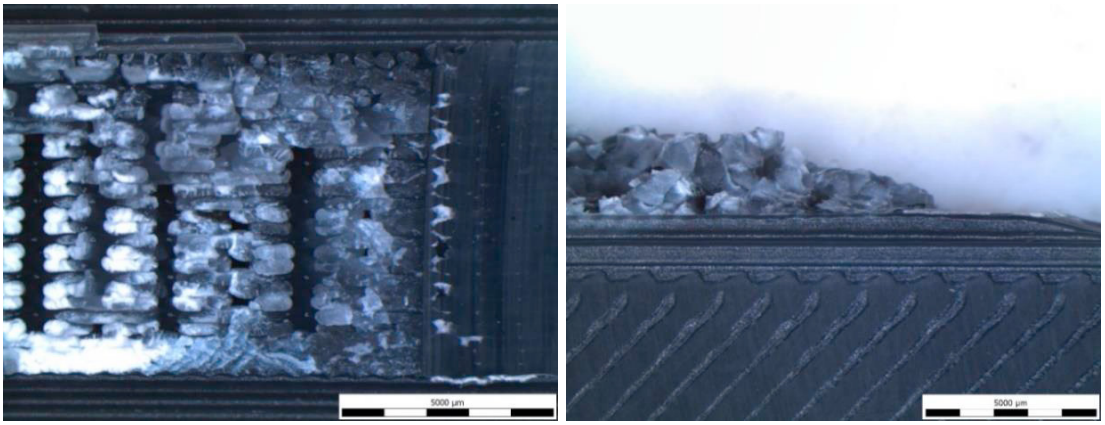

Fig. 5. Fracture surface of 0.3 mm regular CT specimen: Top view (Left); Side view (Right).

The next step was to test the CT specimens with the lower layer height of 0.1 mm. Fracture surfaces of such specimens featured noticeably smoother surfaces and smaller through-thickness holes (Fig. 6-Left). However, the honeycomb inner holes were still present. Fig. 6-Left shows a labeled portion of the final fracture surface (final failure). It is visibly lighter in color compared to the stable crack propagation and there is no difference between layers in terms of crack propagation. Here, lighter regions show the portion of brittle fracture, i.e., the region that failed after the crack length approached the static crack growth limit (the fracture toughness in mode I). Darker regions, on the other hand, show stable, gradual crack propagation in the specimen during fatigue loading. The side view (Fig. 6-Right) shows that there is not such a large difference between the cracks in different layers as in the case of the CT specimens with 0.3 mm layers and that the crack kept a reasonably straight direction even though there are no SGs to assist. Hence, in such specimens, SGs are not needed, because the structural features from AM do not have such a significant effect on the crack propagation direction in the finer printed material.

For additional visualization, there are macroscopic photos of the fractured specimens from the tested batches shown in Fig. 7.

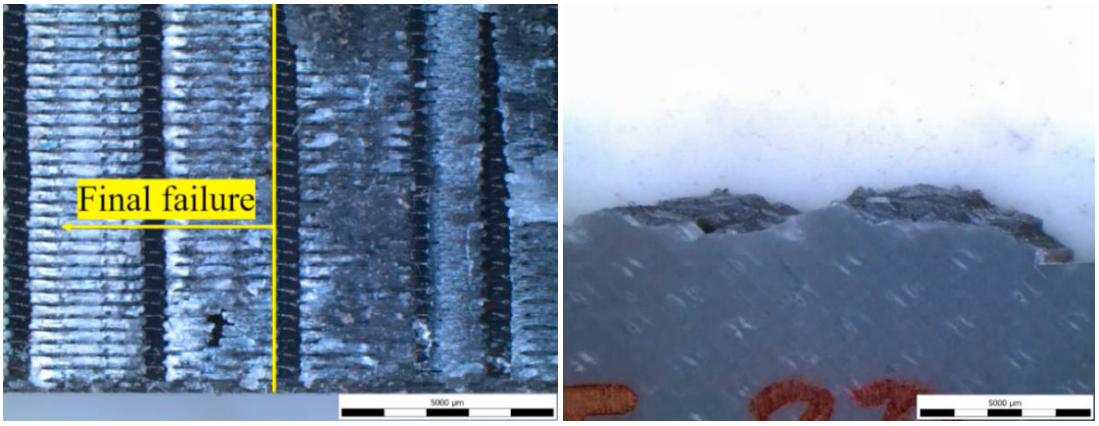

Fig. 6. Fracture surface of 0.1 mm regular CT specimen: Top view (Left); Side view (Right).

Fig. 7. Fractured CT specimens: Regular 0.3 mm (Top); SGed 0.3 mm (Middle); Regular 0.1 mm (Bottom).

The crack kinetics results of all tested CT specimens were fitted with the power equation (Paris' equation), according to Paris & Erdogan (1963):

$$\frac{da}{dN} = C \cdot K_{I,max}^{m} \tag{1}$$

where C and m are material constants (Paris constants) that describe the crack kinetics in the stable crack propagation region, da/dN is the crack growth rate in terms of mm/cycle, and the $K_{I,max}$ is the maximum stress intensity factor in the loading cycle in MPa·m$^{1/2}$. The application of this form of power law on crack propagation in plastics proved plausible, as described in previous works conducted by Arbeiter et al. (2020) and Hutař et al. (2011). The values under 10^{-6} mm/cycle were considered safely under threshold value and were excluded from the fitting.

The data from the 0.3 mm specimens (see Fig. 8-Left) show high data scatter described with an R-square value of 0.3276. As mentioned before, SG CTs had limitations in the data acquisition, therefore in Fig. 8-Left only seven points are presented, but excluded from Paris constants estimation, because of their unreliability. See the results in Table 1.

Table 1. Crack growth kinetics constants for CT specimens with layer heights of 0.3 mm and 0.1 mm.

	Layer height [mm]	
Constant	0.3	0.1
C [-]	$1.6736 \cdot 10^{-4}$	$2.2447 \cdot 10^{-4}$
m [-]	3.8489	3.8449

The advantages of a lower layer height application can be seen in the R-square value for 0.1 mm specimens (see Fig. 8-Right), which is 0.5965. The R-square value is noticeably higher, but it should be even higher for the data to be reliable. See the estimated Paris constants for the 0.1 mm CT specimens in Table 1.

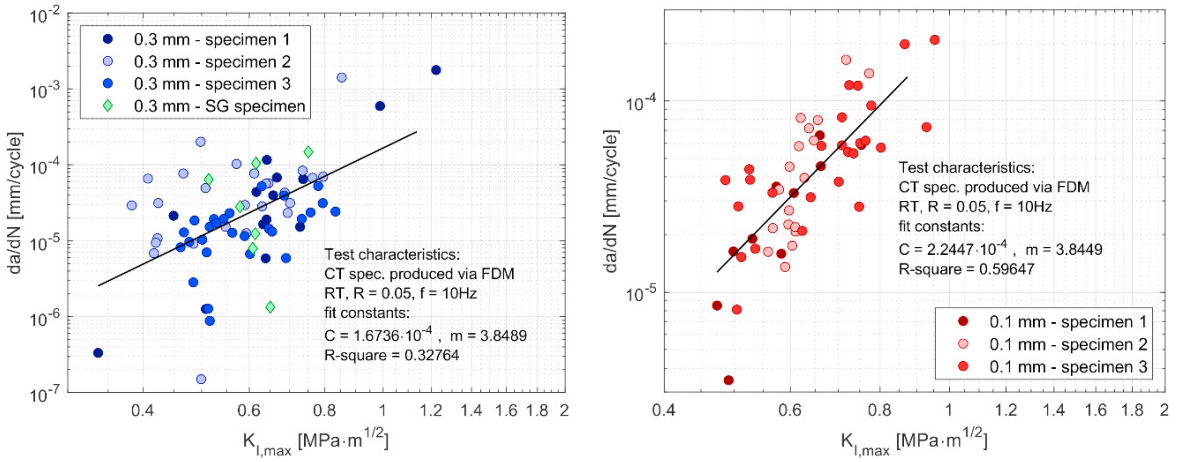

Fig. 8. Crack growth kinetics for 0.3 mm CT specimens (including SG) (Left); Crack growth kinetics for 0.1 mm CT specimens (Right).

The scatter is very high in the case of the 0.3 mm data, which makes it difficult to safely determine the threshold value of $K_{I,max}$. However, it was not possible to see any crack growth below 0.3 MPa·m$^{1/2}$. In the case of the 0.1 mm data, it was observed that the crack growth appears above 0.45 MPa·m$^{1/2}$, but it is necessary to investigate the area of da/dN below 10^{-5} mm/cycle more carefully for more precise assumptions about threshold values. The end of the stable crack growth and transition towards the unstable, rapid crack growth defined by fracture toughness was seen around 1.0 MPa·m$^{1/2}$ for the 0.1 mm specimens and above 0.9 MPa·m$^{1/2}$ for the 0.3 mm. These values suggest that, in general, the finer printed material shows better properties in terms of crack propagation, but more investigations are due in this regard to describe the differences in detail.

4. Conclusions

This paper dealt with experimental crack growth rate investigations in 3D-printed CT specimens made of PLA. The specimens were printed using two different layer heights – 0.1 and 0.3 mm. Also, the effect of printed SGs in the experimental procedure was evaluated.

The first tested CT specimens were regular ones, with 0.3 mm layer height. Here, there is a high crack kinetics data scatter due to specimen inhomogeneity, i.e., the presence of wide holes in the infill structure and different angles of crack propagation between layers (30° for infill structure, 45° for outer layers). In order to force the crack to grow in a straight direction, CT specimens with SGs were tried. SGs proved their intended function, but due to the SG geometry crack inclined to follow the edge of the SG surface, which created an optical barrier for crack observation due to the above layers. The lower material inhomogeneity that was present in the CT specimens with 0.1 mm layer height, i.e., smaller infill holes and better adhesion between the neighboring layers, resulted in a much better performance of these specimens. The crack propagated more or less in a straight direction and there was lower data scatter as a result. It can be concluded that there is no need for SGs on CT specimens with 0.1 mm layer height. The 0.1 mm CT specimens outperformed the 0.3 mm specimens in the crack growth parameters. Threshold values of $K_{I,max.}$ are noticeably higher.

In future work, the suggestion is to improve the SG geometry or specimen preparation for expected irregular crack growth, i.e., crack angulation. The first suggestion is to machine the SG, instead of printing it, because of above layers could influence crack observation. The main issue in AM nowadays is the inhomogeneity of specimen structure. For printing CT specimens, in this research 200 °C extrusion and 100% infill density were applied. Thus, any improvement in the creation of specimens with lower structural inconsistency will lead to an improvement in the accuracy of the collected data and a better comparison of properties achieved with different parameters.

Acknowledgments

The authors would like to thank the support from European Union's Horizon 2020 research and innovation program (H2020-WIDESPREAD2018, SIRAMM) under grant agreement No. 857124.

References

Milovanović, A., Sedmak, A., Grbović, A., Golubović, Z., Mladenović, G., Čolić, K., Milošević, M., 2020. Comparative analysis of printing parameters effect on mechanical properties of natural PLA and advanced PLA-X material. Procedia Structural Integrity 28, pp. 1963-1968. DOI: 10.1016/j.prostr.2020.11.019.

DeStefano, V., Khan, S., Tabada, A., 2020. Applications of PLA in modern medicine. Engineering Regeneration 1, pp. 76-87. DOI: 10.1016/j.engreg.2020.08.002.

Pawar, R.P., Tekale, S.U., Shisodia, S.U., Totre, J.T., Domb, A.J., 2014. Biomedical Applications of Poly(Lactic Acid). Recent Patents on Regenerative Medicine 4 (1), pp. 40-51. DOI: 10.2174/22102965046661404022350 24.

Ebrahimi, F., Dana, H.R., 2022. Poly lactic acid (PLA) polymers: from properties to biomedical applications. International Journal of Polymeric Materials and Polymeric Biomaterials 71:15, pp. 1117-1130. DOI: 10.1080/00914037.2021.1944140.

Petersmann, S., Spoerk, M., Van De Steene, W., Üçal, M., Wiener, J., Pinter, G., Arbeiter, F., 2020. Mechanical properties of polymeric implant materials produced by extrusion-based additive manufacturing. Journal of the Mechanical Behavior of Biomedical Materials 104:103611. DOI: 10.1016/j.jmbbm.2019.103611.

Farah, S., Anderson, D.G., Langer, R., 2016. Physical and mechanical properties of PLA, and their functions in widespread applications — A comprehensive review. Advanced Drug Delivery Reviews 107, pp. 367-392. DOI: 10.1016/j.addr.2016.06.012.

Song, Y., Li, Y., Song, W., Yee, K., Lee, K.Y., Tagarielli, V. L., 2017. Measurements of the mechanical response of unidirectional 3D-printed PLA, Materials & Design 123, pp. 154–164. DOI: 10.1016/J.MATDES.2017.03.051.

Spoerk, M., Arbeiter, F., Cajner, H., Sapkota, J., Holzer, C., 2017. Parametric optimization of intra- and inter-layer strengths in parts produced by extrusion-based additive manufacturing of poly(lactic acid). Journal of Applied Polymer Science 134 (41), pp. 45401. DOI: 10.1002/app.45401.

Ezeh, O. H., Susmel, L., 2018. On the fatigue strength of 3D-printed polylactide (PLA), Procedia Structural Integrity 9, pp. 29–36. DOI: 10.1016/j.prostr.2018.06.007.

Ezeh, O. H., Susmel, L., 2019. Reference strength values to design against static and fatigue loading polylactide additively manufactured with in-fill level equal to 100%. Material Design & Processing Communications 1 (4). DOI: 10.1002/mdp2.45.

Afrose, M. F., Masood, S. H., Iovenitti, P., Nikzad, M., Sbarski, I., 2016. Effects of part build orientations on fatigue behaviour of FDM-processed PLA material, Progress in Additive Manufacturing 1, pp. 21–28. DOI: 10.1007/S40964-015-0002-3.

Jerez-Mesa, R., Travieso-Rodriguez, J.A., Lluma-Fuentes, J., Gomez-Gras, G., Puig, D., 2017. Fatigue lifespan study of PLA parts obtained by additive manufacturing. Procedia Manufacturing 13, pp. 872-879. DOI: 10.1016/j.promfg.2017.09.146.

Travieso-Rodriguez, J.A., Zandi, M.D., Jerez-Mesa, R., Lluma-Fuentes, J., 2020. Fatigue behavior of PLA-wood composite manufactured by fused filament fabrication. Journal of Materials Research and Technology 9(4), pp. 8507–8516. DOI: 10.1016/j.jmrt.2020.06.003.

Zhao, H., Li, L., Ding, S., Liu, C., Ai, J., 2018. Effect of porous structure and pore size on mechanical strength of 3D-printed comby scaffolds. Materials Letters 223, pp. 21-24. DOI: /10.1016/j.matlet.2018.03.205.

Hutmacher, D.W., Schantz, T., Zein, I, Ng, K.W., Teoh, S.H., Tan, K.C., 2001. Mechanical properties and cell cultural response of polycaprolactone scaffolds designed and fabricated via fused deposition modelling. Journal of Biomedical Materials Research 55 (2), pp. 203-216.

Safai, L., Cuellar, J.S., Smit, G., Zadpoor, A.A., 2019. A review of the fatigue behavior of 3D printed polymers. Additive Manufacturing 28, pp. 87-97. DOI: 10.1016/j.addma.2019.03.023.

Gomez-Gras, G., Jerez-Mesa, R., Travieso-Rodriguez, J.A., Lluma-Fuentes, J., 2018. Fatigue performance of fused filament fabrication PLA specimens. Materials & Design 140, pp. 278-285. DOI: 10.1016/j.matdes.2017.11.072.

Alshammari, Y.L.A., He, F., Khan, M.A., 2021. Modelling and Investigation of Crack Growth for 3D-Printed Acrylonitrile Butadiene Styrene (ABS) with Various Printing Parameters and Ambient Temperatures. Polymers 13, 3737. DOI: 10.3390/polym13213737.

Azadi, M., Dadashi, A., Dezianian, S., Kianifar, M., Torkaman, S., Chiyani, M., 2021. High-cycle bending fatigue properties of additive-manufactured ABS and PLA polymers fabricated by fused deposition modeling 3D-printing. Forces in Mechanics 3, 100016. DOI: 10.1016/j.finmec.2021.100016.

Arbeiter, F., Spoerk, M., Wiener, J., Gosch, A., Pinter, G., 2018. Fracture mechanical characterization and lifetime estimation of near-homogeneous components produced by fused filament fabrication. Polymer Testing 66, pp. 105–113. DOI: 10.1016/j.polymertesting.2018.01.002.

Paris, P.C., Erdogan, F., 1963. A Critical Analysis of Crack Propagation Laws. Journal of Basic Engineering 85, pp. 528-533. DOI: 10.1115/1.3656900.

Arbeiter, F., Trávníček, L., Petersmann, S., Dlhý, P., Spoerk, M., Pinter, G., Hutař, P., 2020. Damage tolerance-based methodology for fatigue lifetime estimation of a structural component produced by material extrusion-based additive manufacturing. Additive Manufacturing 36, 1017300. DOI: 10.1016/j.addma.2020.101730.

Valean, C., Marsavina, L., Marghitas, M., Linul, E., Razavi, J., Berto, F., Brighenti, R., 2020. The effect of crack insertion for FDM printed PLA materials on Mode I and Mode II fracture toughness. Procedia Structural Integrity 28, pp. 1134-1139. DOI: 10.1016/j.prostr.2020.11.128.

ASTM D5045-14: Standard Test Methods for Plane-Strain Fracture Toughness and Strain Energy Release Rate of Plastic Materials, (2014).

Gao, G., Xu, F., Xu, J., Tang, G., Liu, Z., 2022. A Survey of the Influence of Process Parameters on Mechanical Properties of Fused Deposition Modeling Parts. Micromachines 13, 553. DOI: 10.3390/mi13040553.

Milovanović, A., Golubovic, Z., Trajkovic, I., Sedmak, A., Miloševic, M., Valean, E., Marsavina, L., 2022. Influence of printing parameters on the eligibility of plane-strain fracture toughness results for PLA polymer, Procedia Structural Integrity 41, pp. 290–297. DOI: 10.1016/J.PROSTR.2022.05.034.

Algarni, M., 2022. Fatigue Behavior of PLA Material and the Effects of Mean Stress and Notch: Experiments and Modeling. Procedia Structural Integrity 37, pp. 676-683. DOI: 10.1016/j.prostr.2022.01.137.

El Magri, A., Vanaei, S., Shirinbayan, M., Vaudreuil, S., Tcharkhtchi, A., 2021. An Investigation to Study the Effect of Process Parameters on the Strength and Fatigue Behavior of 3D-Printed PLA-Graphene. Polymers 12, pp. 3218. DOI: 10.3390/polym13193218.

Hutař, P., Ševčík, M., Náhlík, L., Pinter, G., Frank, A., Mitev, I., 2011. A numerical methodology for lifetime estimation of HDPE pressure pipes. Engineering Fracture Mechanics 78 (17), pp. 3049-3058. DOI: 10.1016/j.engfracmech.2011.09.001.